

OPEN

No Significant Effect of Coulomb Stress on the Gutenberg-Richter Law after the Landers Earthquake

Víctor Navas-Portella^{1,2,3}, Abigail Jiménez⁴  & Álvaro Corral^{1,2,5,6*}

Coulomb-stress theory has been used for years in seismology to understand how earthquakes trigger each other. Whenever an earthquake occurs, the stress field changes, and places with positive increases are brought closer to failure. Earthquake models that relate earthquake rates and Coulomb stress after a main event, such as the rate-and-state model, assume that the magnitude distribution of earthquakes is not affected by the change in the Coulomb stress. By using different slip models, we calculate the change in Coulomb stress in the fault plane for every aftershock after the Landers event (California, USA, 1992, moment magnitude 7.3). Applying several statistical analyses to test whether the distribution of magnitudes is sensitive to the sign of the Coulomb-stress increase, we are not able to find any significant effect. Further, whereas the events with a positive increase of the stress are characterized by a much larger proportion of strike-slip events in comparison with the seismicity previous to the mainshock, the events happening despite a decrease in Coulomb stress show no relevant differences in focal-mechanism distribution with respect to previous seismicity.

Since the LAquila event in 2009 seismologists have advocated the modeling and testing of earthquakes within a rigorous statistical framework¹, following on the CSEP (Collaboratory for the Study of Earthquake Predictability) previous works. A recent pseudo-prospective forecast was conducted on the 2010–2012 Canterbury, New Zealand, series, in order to test a total of fourteen earthquake models^{2,3}. Its results offer some encouragement for a physical basis in earthquake forecasting and suggest that some of the recent physics-based and hybrid model development have added informative components⁴.

Our basic understanding of earthquake physics is that stress is being accumulated on certain regions due to different mechanisms, and that those regions rupture whenever that stress surpasses the strength of the material. That rupture is the earthquake. The mechanisms by which stresses change are diverse: in addition to tectonic driving, they can be induced by precedent earthquakes^{5–9}, by volcanic activity¹⁰, or even by artificial means, such as injection of fluids¹¹ or aquifer withdrawal¹². Coulomb-stress theory has been used to forecast spatial patterns of aftershock rates, as well as assessing the likelihood of earthquake rupture sequences^{13,14}. Although there exist instances where its predictive skills are arguable^{15–18}, the monitoring of the changes in the stress field represents a valuable information for seismic and volcanic hazard forecasting and to proposing the adequate mitigation measures.

A hallmark of statistical seismology and of earthquake hazard assessment is the well-known Gutenberg-Richter relation, or Gutenberg-Richter law^{19–21}. This law states that earthquake magnitudes must be described in terms of a probability distribution and that, above a lower cut-off value, this distribution is exponential. In terms of the probability density $f(m)$ one has

$$f(m) = (b \ln 10) 10^{-b(m-m_{\min})} \propto 10^{-bm},$$

defined for $m \geq m_{\min}$ (values below m_{\min} are disregarded), with m the magnitude, m_{\min} the lower cut-off in magnitude, b the so called b -value (directly related to the exponent β of the power-law complementary cumulative distribution of seismic moment, $\beta = 2b/3$), and the symbol \propto denoting proportionality. This relation is usually

¹Centre de Recerca Matemàtica, Edifici C, Campus Bellaterra, E-08193, Barcelona, Spain. ²Barcelona Graduate School of Mathematics, Edifici C, Campus Bellaterra, E-08193, Barcelona, Spain. ³Facultat de Matemàtiques i Informàtica, Universitat de Barcelona, Barcelona, Spain. ⁴Departamento de Computación e Inteligencia Artificial, Universidad de Granada, Campus Ceuta, Cortadura del Valle s.n., E-51001, Ceuta, Spain. ⁵Departament de Matemàtiques, Universitat Autònoma de Barcelona, E-08193, Barcelona, Spain. ⁶Complexity Science Hub Vienna, Josefstädter Straße 39, 1080, Vienna, Austria. *email: alvaro.corral@uab.es

called magnitude-frequency distribution in seismology. A straightforward property of the exponential distribution leads to the fact that the rate (the number per unit time of earthquakes above a certain magnitude m) is also a decreasing exponential function of the magnitude, with the same b -value.

Earthquake hazard forecasts usually comprise two stages: in the first one, the rate of events is forecasted, while in the second one, the Gutenberg-Richter law is applied to those rates in order to obtain the probabilities of occurrence for each magnitude threshold. In the case of physics-based models, the forecasted rates of events depend on the Coulomb stresses calculated in the region of interest. These models are variants of the rate-and-state model by Dieterich²²,

$$R(t) = r[1 + (e^{-\Delta CFS/B} - 1)e^{-t/t_a}]^{-1} \quad (1)$$

where $R(t)$ is the rate of events (i.e., aftershocks) at any given time t after a mainshock, r is the rate of background seismicity, ΔCFS is the increase in Coulomb stress induced by the mainshock, B is a constant, for our purposes, and t_a is the characteristic relaxation time²².

Note that in the application of the Gutenberg-Richter law to the forecasted rate $R(t)$ given by the previous expression it is implicit that the Coulomb-stress change caused by a mainshock does not alter the fulfillment of the Gutenberg-Richter law for the aftershocks, in particular, this law remains the same no matter whether ΔCFS is positive or negative. In some sense, $R(t)$ inherits the dependence of the background rate r with the magnitude. Therefore, the rate-and-state formulation^{14,22–26} assumes the fulfillment of the Gutenberg-Richter law for the incoming events (aftershocks), with no change in the b -value. This assumption is made when inverting earthquake rates to obtain stress changes^{10,27,28}. Physics-based models also assume the magnitude distribution does not depend on the stress values, so that forecasted rates can be translated into probabilities of occurrence for different magnitudes.

In fact, it has been long debated²⁹ whether the value of b in the Gutenberg-Richter law is essentially universal²¹ or whether, on the contrary, it is affected by different geophysical conditions^{30–32}. Some studies^{30,31} have correlated the b -value (and also the parameters of the Omori law^{33–35}) with the style of faulting³⁶. These studies indicate that (at least for California, for a long time period) $b \approx 1.03$ for normal events, $b \approx 0.87$ for strike-slip events, and $b \approx 0.79$ for thrust events³⁰. As the b -value is directly related to the log-ratio between the number of small and large earthquakes, variations in b can be associated with the ability of an earthquake rupture to propagate (more large events, low b) or not (less large events, high b).

According to Mohr-Coulomb theory^{31,37}, thrust faults rupture at much higher Coulomb stress than normal faults (with strike-slip faults in between, assuming the same value for the coefficient of static friction). When the stress required to initiate a rupture is higher, stress interactions are enhanced and cracks can propagate faster in many different directions, yielding larger earthquakes³¹, consistent with the empirically observed b -values for thrust faulting³⁰. Conversely, for lower rupture thresholds, one should find indeed the large b -values characterizing normal faulting. Although the threshold for triggering might be different for the different styles of faulting, the rupture or not of a fault also depends on its previous state.

Here we investigate, with rigorous statistical tools, if the Gutenberg-Richter law is affected by the binary choice between positive and negative increases of the Coulomb stress, using the sequence of aftershocks after the 1992 Landers earthquake. This event is chosen for illustration due to its particular relevance, as it yields one of the most studied mainshocks and aftershock sequences in the history of seismology; nevertheless, we are equally interested in developing the methodological aspects to approach this problem. The next section explains the seismic catalog and the spatio-temporal window used to define this sequence. Section 3 develops the procedure to calculate the increase in the Coulomb stress that the Landers earthquake provokes in the fault plane of each event in the sequence. The statistical analysis is also exposed in this section. Section 4 presents the results and section 5 summarizes the conclusions. We anticipate that the number of Landers aftershocks in the relevant window of space, time, magnitude, and Coulomb-stress increase is too low to reach statistically significant results. We suspect this may be a general characteristic of many other important aftershock sequences.

Data

The June 28, 1992, Landers earthquake, with a moment magnitude $m = M_w = 7.3$ and a rake angle $\rho = -177^\circ$, corresponding to strike-slip focal mechanism, has been the strongest one in Southern California at least since 1952. The earthquake and its subsequent aftershock sequence have been extensively studied^{38–40}, with a number of slip distributions that describe its rupture^{41–44}. In this work we use four slip models to calculate the strain; these models are: Wald and Heaton (referred here to as **wald**)⁴¹, Hernandez *et al.* (**hernandez**)⁴², Landers Big-Bear California (**bbcal**)⁴³ and Landers Surface Rupture (**surfrup**)⁴⁴. The terminology is the same as the one used in ref.⁴³

High quality catalogs for Southern California are nowadays available^{45,46}; in particular in this paper we will select the Landers' aftershocks from the Yang-Hauksson-Shearer (YHS) catalog⁴⁷, which incorporates focal-mechanism solutions. Given the distribution of acceptable mechanisms, the preferred solution is the most probable one⁴⁸. The ambiguity of the actual fault plane is solved by considering that the preferred nodal planes are those associated with the preferred solution listed in the catalog⁴⁷. The focal mechanism, in concrete, the rake angle, together with Landers stress field derived from the slip model, allows us to calculate Coulomb-stress increases (positive or negative) induced by the mainshock on the actual orientations of the aftershock fault planes. Nevertheless, if one does not trust the preferred solutions reported in the catalog, an alternative procedure can be applied based on selecting the nodal plane in which the Coulomb stress increase is maximum⁴⁹. Note that the YHS catalog does not report the moment magnitude necessarily but a preferred magnitude.

In order to better detect the influence of the Landers stress change we take a time window of 100 days after the mainshock and a spatial window going from 10 to 150 km from the mainshock rupture. The time of occurrence

of the Landers earthquake is taken as the time origin except for the bbcal slip model where the time origin is set by the Big-Bear earthquake (which occurred approximately three hours after Landers earthquake with a moment magnitude $m = M_w = 6.3$ and rake angle $\rho = -180^\circ$ ⁴³). We tried other choices for the limits of the window finding similar results as reported in the Supplementary Material. The referred spatio-temporal window defines Landers aftershocks for our purposes. Distances to the Landers rupture are computed as the minimum Euclidean distance from the aftershock hypocenter to the center of each rupture patch as given by the slip model. The reason to exclude events closer than 10 km is the uncertainty of the deformation field near the edges of the subfaults⁵⁰, as the finite-fault approximation provides spurious values near the fault zone because of boundary effects.

Procedure

Continuum mechanics. The dMODELS software in ref. ⁵¹ calculates the deformation field (or displacement) caused by different models corresponding to different physical processes. Although there exist many programs that calculate deformation caused by earthquakes, this package has been thoroughly tested, and can introduce many different sources of deformation, which can be translated into stress changes in a straightforward way. The dMODELS software will be the one used here to obtain deformation field from the different slip models of Landers.

The local coordinate system for dMODELS is east-north-up, ENU. After introducing the corresponding slip model (also called source model) for the mainshock of interest (Landers in our case⁴³) into the dMODELS program we obtain the projections in the ENU axes of the deformation field \vec{u} caused by the mainshock at the position of each aftershock (and also at its neighborhood, in order to take spatial derivatives). We then obtain the strain tensor associated to \vec{u} by calculating the (symmetrized) gradient of the deformation⁵², whose components are $\varepsilon_{ij} = (\nabla_i u_j + \nabla_j u_i)/2$ (with a spatial step equal to 1 km).

Afterwards, we assume an isotropic and elastic material for calculating the stress tensor⁵², or, more precisely, the contribution of the mainshock to the stress tensor, $s_{ij} = 2\mu\varepsilon_{ij} + \lambda\delta_{ij}\sum_k \varepsilon_{kk}$, with δ_{ij} the components of the identity matrix and with the Lamé elastic moduli given by $\mu = \lambda = 3 \times 10^4$ MPa³⁷ (Poisson ratio $\nu = \lambda(\lambda + \mu)^{-1}/2 = 0.25$). Moreover, when calculating the stress induced by previous events (mainshocks) on new events (aftershocks) it is necessary to orientate it onto the aftershock fault planes^{53,54}, so that one can actually evaluate if the new events could have been triggered by the induced stress or not. Given the fault plane and slip vector of an aftershock, we calculate the change in the normal σ_n and shear (or tangential) τ stresses in that orientation and position, as

$$\Delta\sigma_n = \sum_{ij} n_i s_{ij} n_j \text{ and } \Delta\tau = \sum_{ij} \ell_i s_{ij} n_j, \quad (2)$$

with n_i and ℓ_i the components of the normal and slip vectors, respectively. The formulas to obtain the ENU components of these vectors from the information recorded in the YHS catalog (strike, dip and rake angles⁵⁵) are given in the Methods section. Our calculation of the Coulomb-stress changes over the planes of the actual faults⁵³ is in contrast with an approach in which Coulomb stresses are calculated onto the so-called optimally oriented planes⁶, when the only information available is the regional stress. However, optimally oriented planes are imaginary planes that might not correspond to the actual geology, and thus, our approach is more realistic.

The Mohr-Coulomb failure criterion⁵⁶ states that the shear stress τ on a fault that ruptures must surpass the critical value τ_c , which is a linear function of the normal stress,

$$\tau_c = C - \mu'\sigma_n \quad (3)$$

with C the cohesion and μ' the effective fault friction coefficient (including the contribution of the pore pressure^{6,57}). Care must be taken with the convention of signs in the normal stress, which is not the same in geophysics than in solid mechanics (our convention takes the negative sign for compression, this is the reason for the negative sign before μ'). From this failure criterion it is natural to define the Coulomb stress as

$$CFS = \tau + \mu'\sigma_n, \quad (4)$$

which signals failure by $CFS > C$. In fact, for pre-existing faults one can consider that the cohesion is nearly zero. In any case, the change in Coulomb stress at the aftershock fault plane due to the mainshock will be

$$\Delta CFS = \Delta\tau + \mu'\Delta\sigma_n, \quad (5)$$

with $\Delta\tau$ and $\Delta\sigma_n$ coming from Eq. (2). Thus, positive increases of the Coulomb stress bring the fault closer to failure, whereas negative increases distance it away from failure. As the real value of the effective friction coefficient μ' is uncertain³⁷, we will check different values of it as in ref. ¹⁵.

In Fig. 1 we present a scatter plot that shows the resulting absolute values of the increase of Coulomb stress $|\Delta CFS|$ over each aftershock and their dependence with the distance between the aftershock and the Landers rupture for the four slip models. As it is implicit by the Coulomb theory, the value of the increase of Coulomb stress decays as the cube of the distance to the rupture. In Figs. 2, 3 and 4 we show aftershocks with strike-slip, normal and thrust focal mechanisms respectively for $m \geq 4$ and positive and negative ΔCFS , as calculated from the hernandez slip model. The same figures including aftershocks with magnitude larger than 3 are shown in the Supplementary Material.

Statistical methods. Once we know the Coulomb-stress change in the fault plane of each aftershock we can separate these into two subsets attending to the value of the change, with the most natural separation being between positive and negative increases (denoted by sub-indexes $>$ and $<$, respectively). Naturally, we expect to

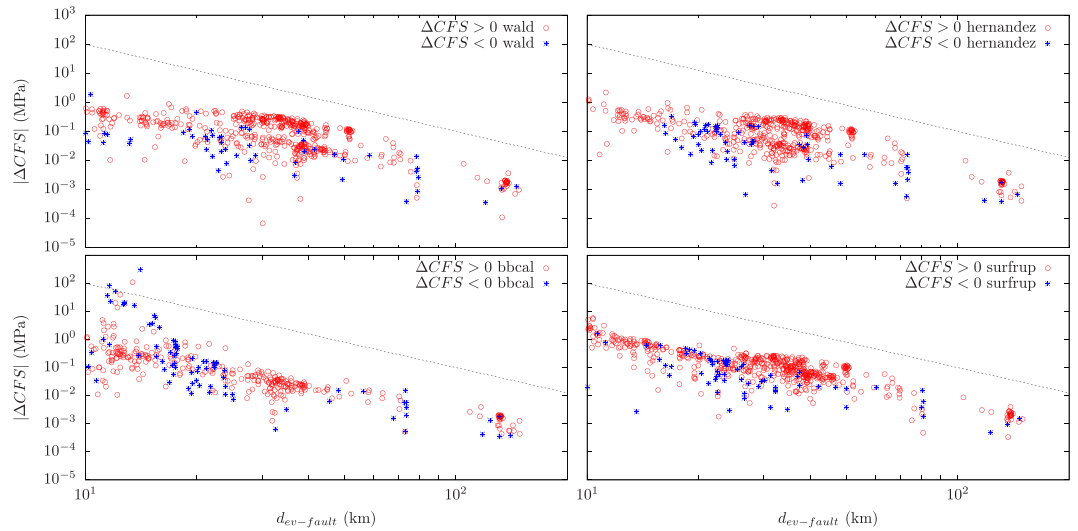


Figure 1. Dependence of the absolute value of the change in the Coulomb stress ΔCFS as a function of the distance of the aftershocks to the Landers rupture for each slip model, with $\mu' = 0.4$ and $m \geq 3$. Aftershocks correspond to the first 100 days after the mainshock and distance is restricted to the range from 10 to 150 km. Black dashed line with slope -3 , as stated by Coulomb theory, is shown as a guide to the eye.

obtain many more aftershocks with positive ΔCFS than with negative ΔCFS ⁵⁸. It is for each of these subsets that we will study the fulfillment of the Gutenberg-Richter law. For any set or subset (or sub-catalog) of earthquakes, the value of b in the Gutenberg-Richter law can be automatically obtained by maximum-likelihood estimation, as^{59,60}:

$$b = \frac{\log_{10} e}{\bar{m} - m_{min}}, \tag{6}$$

with \bar{m} the mean magnitude of the events considered (i.e., those above m_{min}). Let us stress that m_{min} is not the minimum magnitude recorded in the catalog but the value from which we fit the Gutenberg-Richter law to the data. As the resolution of the magnitude Δm is small ($\Delta m = 0.01$) it is not necessary to perform the discreteness correction⁶¹.

In principle, results should not significantly depend on the value of m_{min} , but the larger its value the less data to calculate the b -value and the larger the uncertainty, whereas for a too small m_{min} the Gutenberg-Richter law would not be fulfilled due to the incompleteness of the catalog and the resulting b -value would be artefactual. In this paper we have taken $m_{min} = 3$, which ensures the fulfillment of the Gutenberg-Richter law for all data sets analyzed, as we have verified by means of the Kolmogorov-Smirnov goodness-of-fit test⁶², where the distribution of the test statistic and, from it, the p -value of the fit, p_{fit} , is calculated using 10^4 Monte Carlo simulations^{63,64}. Although some fitting procedures look for the value of m_{min} that optimizes the fit for a given data set⁶³⁻⁶⁵, we have opted for a fixed m_{min} in order to compare the different subsets on the same footing. So, in all cases the exponential fit for $m \geq 3$ cannot be rejected (p_{fit} larger than 0.05). Note that m_{min} defined in this way can be considered a magnitude of completeness, and thus, our value of m_{min} turns out to be rather conservative or strict, in the sense that it is larger (and therefore safer) than in other works⁶⁶.

The maximum-likelihood estimation of the b -value has an associated uncertainty given by its standard deviation

$$\sigma = \frac{b}{\sqrt{N}},$$

where N is the number of earthquakes with $m \geq m_{min}$ in the subset, out of a total number N_{tot} (of any magnitude)⁶⁷. Note that this uncertainty only depends on the number of data, and has nothing to do with the goodness of the fit. This result, as well as the formula for the maximum-likelihood estimation of b , Eq. (6), can also be obtained from ref. ⁶⁴ just taking into account the relation between moment magnitude and seismic moment. The standard deviation, σ , is what represents the uncertainty when we report our resulting b -values.

The comparison between the b -values of the subsets with different values of ΔCFS is done by means of the following statistic

$$z = \frac{b_{>} - b_{<}}{\sqrt{\sigma_{>}^2 + \sigma_{<}^2}} = \frac{b_{>} - b_{<}}{\sqrt{b_{>}^2/N_{>} + b_{<}^2/N_{<}}},$$

where the sub-indexes $>$ and $<$ refer to positive and negative increases of the Coulomb stress. This statistics is rooted on the null hypothesis that both subsets of data (positive and negative) belong to the same underlying

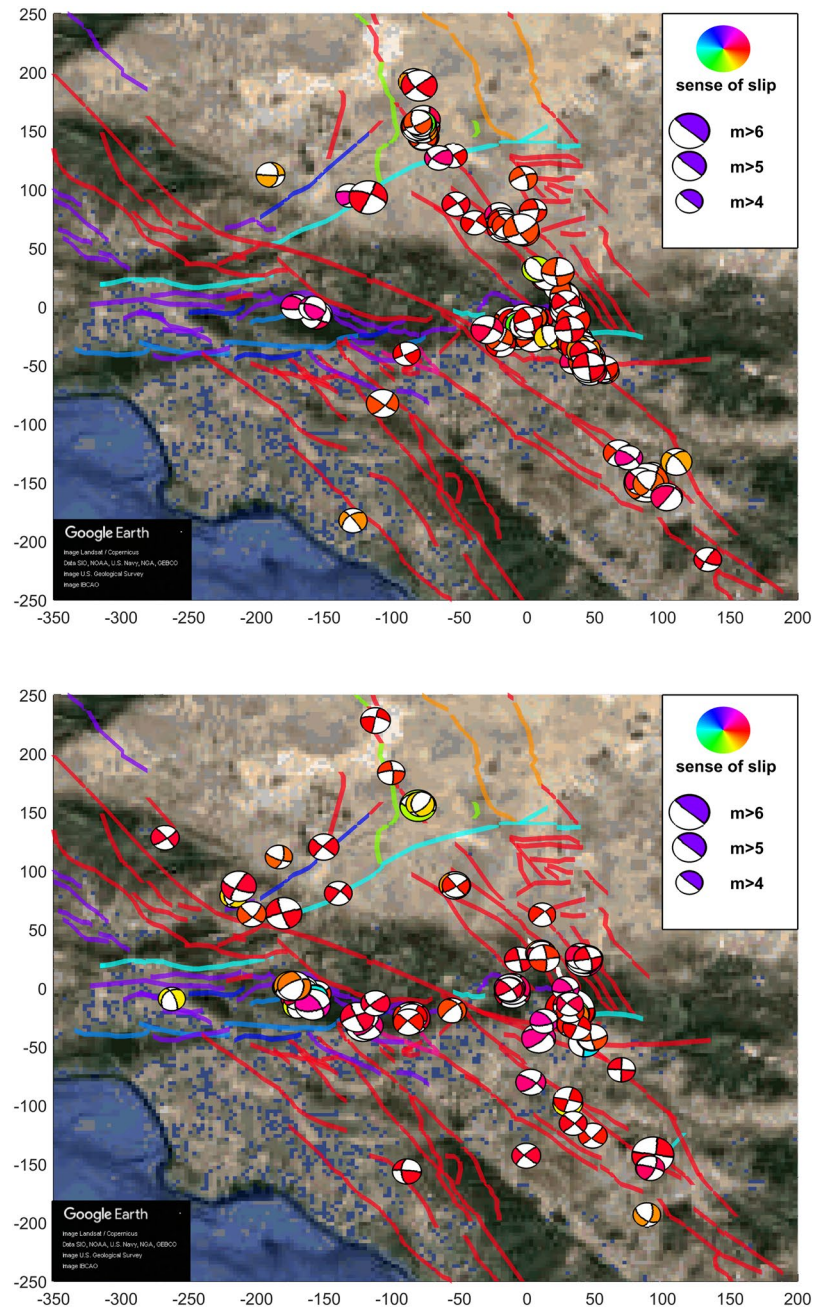


Figure 2. Focal mechanism representation for strike-slip Landers aftershocks, separated in terms of ΔCFS , as calculated from the hernandez slip model (time window of 100 days after the mainshock). Top: $\Delta CFS > 0$. Bottom: $\Delta CFS < 0$. Color scale represents the sense of slip (rake) and fault traces are also shown using the same color code: red for right-lateral (ρ close to $\pm 180^\circ$), light blue for left-lateral (ρ close to 0°), green for normal (ρ close to -90°) and dark blue or purple for thrust faulting (ρ close to 90°). An area of 550×500 km is shown; aftershocks are restricted to $m \geq 4$ (for clarity sake). Aftershocks beyond the limit of 150 km are also shown. Both axes display distances with respect an arbitrary origin, in km.

population of earthquake magnitudes and then, both estimators of the b -value ($b_>$ and $b_<$) have a common mean value, which is that of the whole population. Therefore, under the null hypothesis, $b_> - b_<$ has zero mean and standard deviation $\sqrt{\sigma_>^2 + \sigma_<^2}$ (approximating the population variance from the sample values of $b_>$ and $b_<$ and assuming zero covariance between $b_>$ and $b_<$) and then z has zero mean too and unit standard deviation. An additional assumption is that z is normally distributed, which is supported by theory in the asymptotic limit ($N_>$ and $N_<$ going to infinity⁶⁸). Assuming normality we will test the null hypothesis just comparing the value of z with the standard normal distribution and the hypothesis will be rejected if the value of z is too extreme for a given

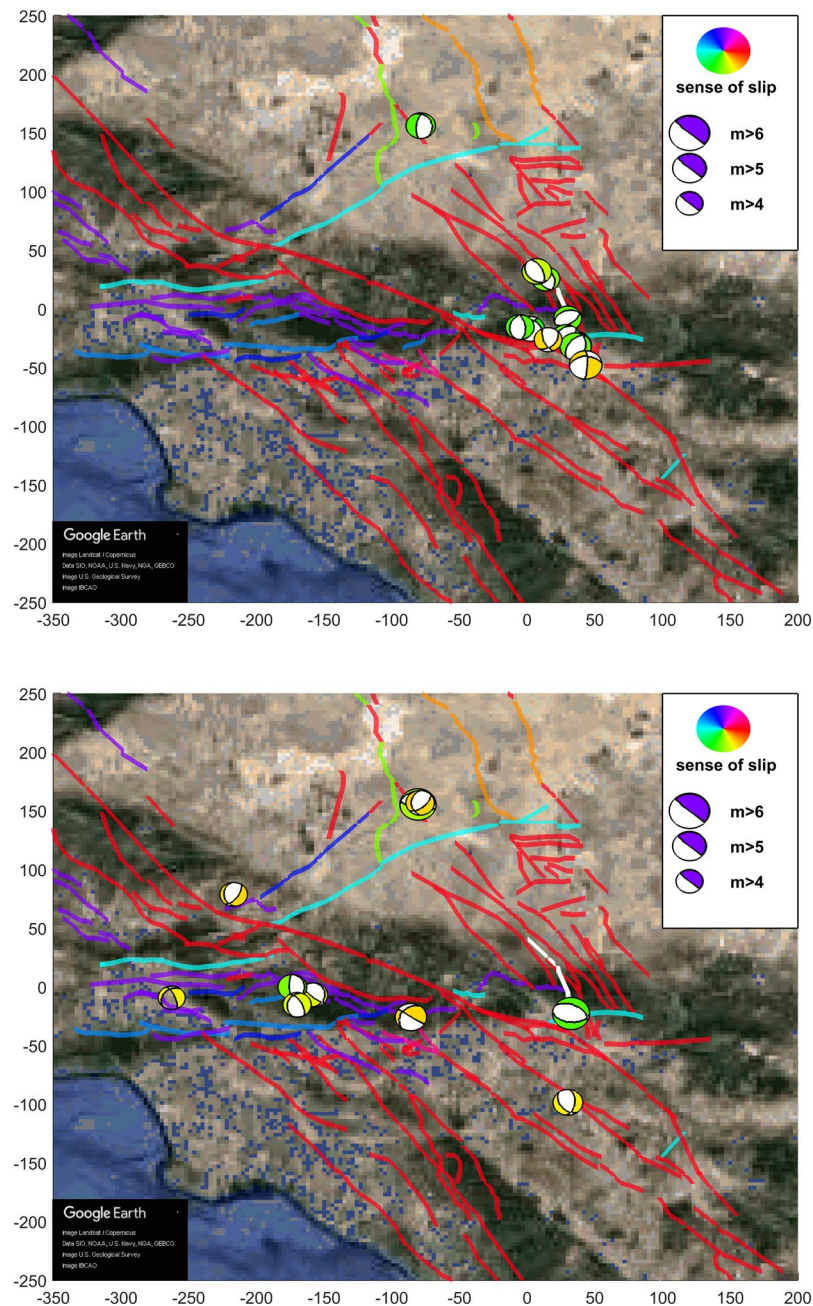


Figure 3. Same as previous figure, for aftershocks with normal focal mechanism.

significance level; in quantitative terms this will be given by a p – value, called p_{norm} , smaller than the significance level (0.05, let us say; corresponding to 0.95 confidence).

If we do not want to believe that the asymptotic regime has been reached the best option is to use a permutation test⁶⁹. Under the null hypothesis (same underlying population of magnitudes) one is allowed to aggregate both subsets (positive and negative) and take, without repetition, two sub-samples of size $N_>$ and $N_<$; note that this is equivalent to take a permutation of the aggregated sample and separate it into two parts ($>$ and $<$). One proceeds in the same way as in the original data, calculating (by maximum likelihood) $b_>^*$, $b_<^*$, and from here $\sigma_>^*$, $\sigma_<^*$, and z^* , where the asterisk marks that we are dealing with a permutation of the original data. Repeating the permutation procedure many times we find the distribution of z^* , which can be compared with the original value z . The p – value of the permutation test, p_{perm} , will be given by the fraction of permutations for which $|z^*|$ is larger than $|z|$ (the empirical value). In our case we take 10^4 permutations.

As a complement, instead of the fitted b -values we may directly compare the distributions; this can be done with the two-sample Kolmogorov-Smirnov test, whose null hypothesis is that both data sets come from the same population, so, the two empirical distributions ($>$ and $<$) are two realizations of a unique theoretical distribution (which remains unveiled)⁶². This test leads to a p -value that we call p_{2ks} . A final comparison comes from the

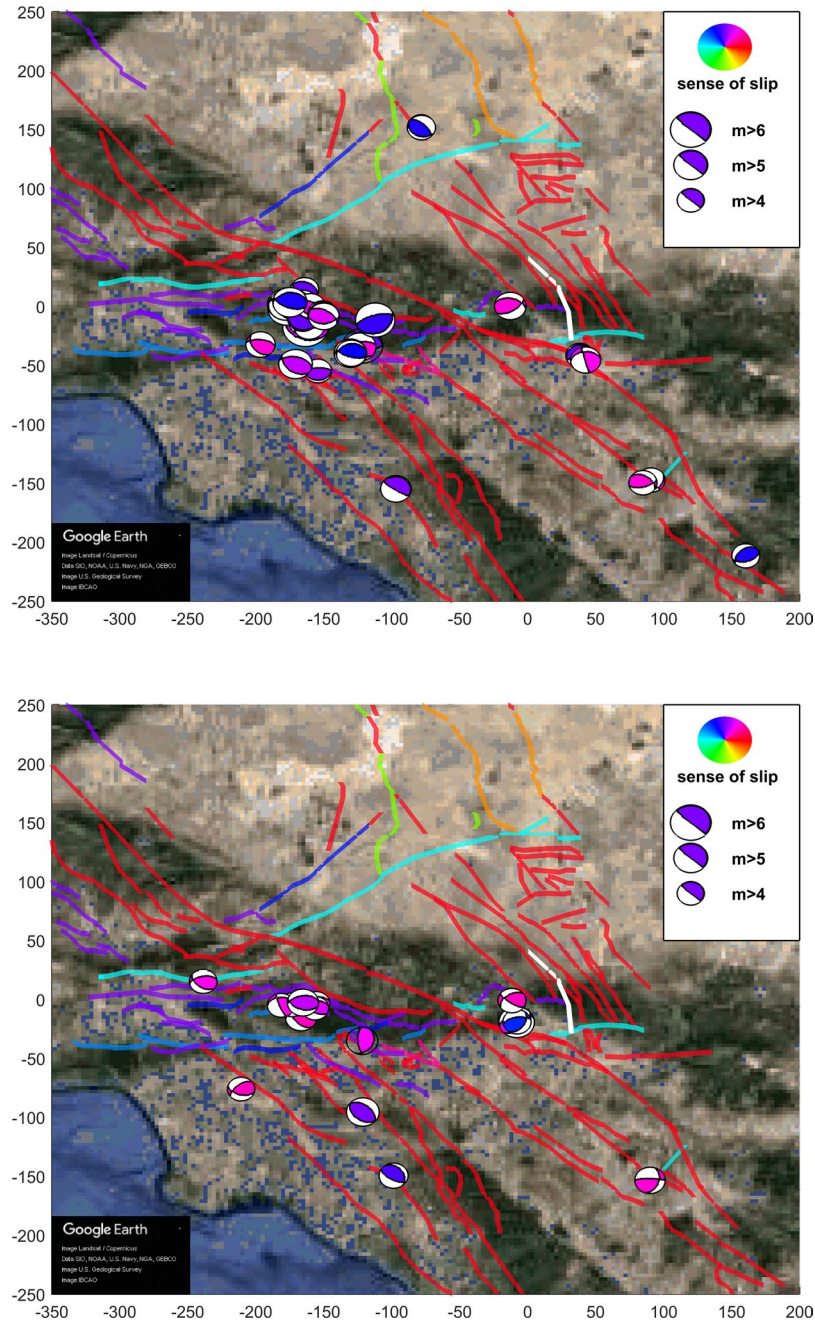


Figure 4. Same as previous figure, for aftershocks with thrust focal mechanism.

application of the Akaike information criterion (AIC)⁷⁰. We consider that we aggregate both subsets (positive and negative ΔCFS) but keeping the distinction in the sign of ΔCFS . Then, we contemplate two options. Model 1, simple: we fit the aggregated data set with one single Gutenberg-Richter exponential leading to the value b_{all} . Model 2, “complex”: we fit each data set with its own exponential function (values $b_{>}$ and $b_{<}$). In each case, $AIC = 2k - 2\hat{\ell}$, where k is the number of parameters of each model and $\hat{\ell}$ is the log-likelihood of the model at maximum. The likelihood in model 2 is the sum of likelihoods for each subcatalog⁶⁸. The model yielding the smallest AIC should be preferred. Defining $\Delta AIC = AIC_2 - AIC_1$ leads to the rejection of the simple model when ΔAIC is significantly below zero (see next section).

Results

Table 1 shows the values of b obtained from the application of the maximum-likelihood-estimation procedure explained above to the different subcatalogs obtained from the Landers sequence. We can see how, in the overall case (when events are not separated in terms of Coulomb-stress change), the Gutenberg-Richter law is fulfilled with an average value $b_{all} = 0.92$. Each slip model leads to a different value of b_{all} because the fault geometry is

Slip model		N_{tot}	N	b -value	σ	p_{fit}
wald	$\Delta CFS > 0$	5213	509	$b_{>} = 0.927$	0.041	0.313 ± 0.005
	$\Delta CFS < 0$	814	51	$b_{<} = 0.766$	0.107	0.861 ± 0.003
	All	6027	560	$b_{all} = 0.909$	0.038	0.243 ± 0.004
hernandez	$\Delta CFS > 0$	5027	465	$b_{>} = 0.926$	0.043	0.505 ± 0.005
	$\Delta CFS < 0$	765	62	$b_{<} = 0.866$	0.110	0.197 ± 0.004
	All	5792	527	$b_{all} = 0.919$	0.040	0.231 ± 0.004
bbcal	$\Delta CFS > 0$	3641	309	$b_{>} = 0.978$	0.056	0.232 ± 0.004
	$\Delta CFS < 0$	1191	82	$b_{<} = 0.948$	0.105	0.327 ± 0.005
	All	4832	391	$b_{all} = 0.971$	0.049	0.053 ± 0.002
surfrup	$\Delta CFS > 0$	5534	548	$b_{>} = 0.890$	0.038	0.290 ± 0.005
	$\Delta CFS < 0$	774	68	$b_{<} = 0.891$	0.108	0.555 ± 0.005
	All	6308	616	$b_{all} = 0.890$	0.036	0.239 ± 0.004

Table 1. Results of fitting the Gutenberg-Richter law to the Landers aftershocks, separating positive and negative Coulomb-stress increases, for different slip models, $\mu' = 0.4$, and $m_{min} = 3$. Aftershocks correspond to the first 100 days after the Landers mainshock and their distance to the Landers rupture is restricted to be between 10 and 150 km. The p -value of the goodness-of-fit test is computed with 10^4 simulations and is denoted by p_{fit} . Its uncertainty corresponds to one standard deviation. In no case the Gutenberg-Richter law can be rejected.

Slip model	z	p_{norm}	p_{perm}	d_{2ks}	p_{2ks}	ΔAIC
wald	1.396	0.163	0.156 ± 0.004	0.139	0.311	0.234
hernandez	0.511	0.609	0.596 ± 0.005	0.095	0.690	1.748
bbcal	0.254	0.800	0.828 ± 0.004	0.063	0.952	1.936
surfrup	-0.010	0.992	0.994 ± 0.001	0.094	0.643	1.999

Table 2. Results of the statistical tests comparing b -values and magnitude distributions for positive and negative Coulomb-stress changes, using different slip models and $\mu' = 0.4$ (same data as previous table). Columns 2 to 4: testing the null hypothesis that there is no difference between the b -values (i.e., $b_{>} = b_{<}$). Both asymptotic normality of the z statistic and a permutation test are used for the calculation of the p -value (labeled as p_{norm} and p_{perm} , respectively). In the latter case the number of permutations is 10^4 , and the uncertainty of p_{perm} corresponds to one standard deviation. Columns 5 to 6: testing the null hypothesis that there is no difference in the distributions, using the 2-sample Kolmogorov-Smirnov test. d_{2ks} and p_{2ks} are the 2-sample Kolmogorov-Smirnov statistic and its p -value. Values of $\Delta AIC = AIC_2 - AIC_1$ are also included in the last column.

different, and events too close to the fault are discarded. This b -value for the Landers aftershocks is found, not surprisingly, to be close to the average for aftershocks in California, $b \simeq 0.9^{71,72}$, and somewhat below the long-term value of Southern California (all events), $b \simeq 1.0^{73}$ (although other works report $b \simeq 1.0$ for Landers aftershocks, probably due to the consideration there of a much smaller magnitude of completeness⁷⁴).

Comparison of distributions. After separating by the sign of the Coulomb-stress change, the first result that becomes apparent from Table 1 is that the number of aftershocks with positive increases is much larger than the number for the negative case^{6,7}, no matter the slip model used to calculate ΔCFS . Regarding the b -values, although they depend on the slip model, we can summarize them by taking the mean of the four models, which, for $\mu' = 0.4$, is $b_{>} \simeq 0.93$ and $b_{<} \simeq 0.87$ with individual uncertainties around 0.04 and 0.11 respectively. Note that the magnitude distribution for the overall case is a mixture of the distributions corresponding to $\Delta CFS > 0$ and $\Delta CFS < 0$, and therefore, the value of b in the overall case turns out to be the harmonic mean of $b_{>}$ and $b_{<}$, i.e.,

$$b_{all}^{-1} = \frac{N_{>} b_{>}^{-1} + N_{<} b_{<}^{-1}}{N_{>} + N_{<}} \quad (7)$$

see refs. ^{75,76}. In order to properly compare the values of $b_{>}$ and $b_{<}$, statistical testing becomes necessary⁷⁷.

Table 2 compares $b_{>}$ and $b_{<}$ for the different slip models taking $\mu' = 0.4$, and shows that the difference in the b -values can not be considered significantly different from zero with a confidence larger than 0.95 so, the null hypothesis $b_{>} \simeq b_{<}$ can not be rejected. This result is true for all the statistical tests as all the p -values (p_{norm} and p_{perm}) are greater than 0.05. Table 2 also shows the results of the two-sample Kolmogorov-Smirnov test and the calculation of ΔAIC leading in both cases to the result that no change in the distributions as a function of positive and negative ΔCFS can be established. In concrete, ΔAIC is always greater than the critical value $\Delta AIC_c = -1.84^{70,78}$ at significance level of 0.05, so the simple model with a unique exponent b_{all} is preferred. The wald slip model is the one for which both distributions (positive and negative) appear as more different; however, the difference is not significant. Figure 5 shows the probability density functions as well as the complementary cumulative distribution functions in this case. Similar results are found when, instead of using the solutions

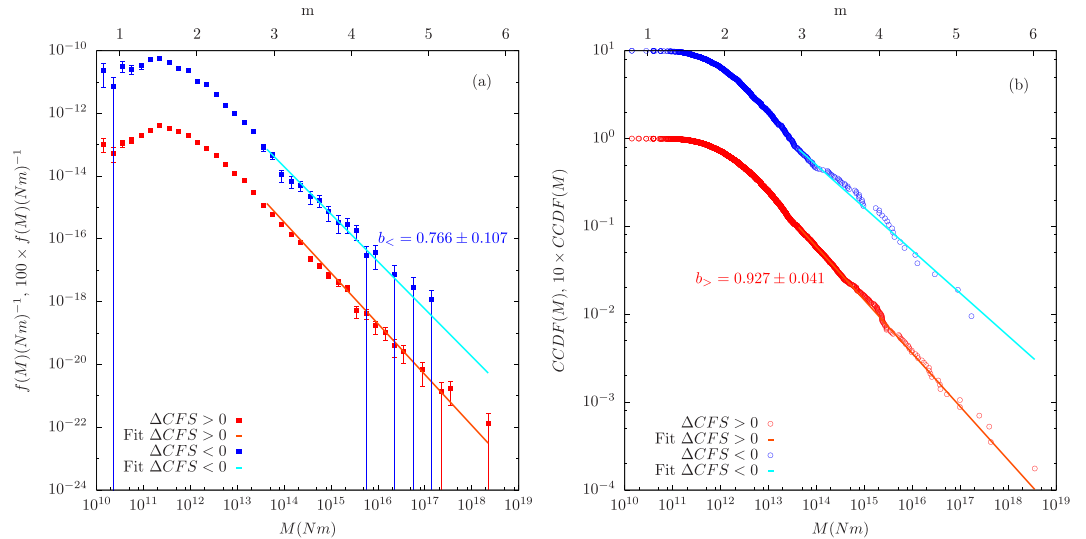


Figure 5. Estimation of the probability densities (a) and of the complementary cumulative distribution functions (CCDF) (b) of seismic moment M separating in terms of $\Delta CFS > 0$ and $\Delta CFS < 0$ for Landers aftershocks during 100 days using the wald slip model and $\mu' = 0.4$. Curves corresponding to $\Delta CFS < 0$ have been conveniently multiplied by a factor 100 and 10, respectively, for clarity sake. Error bars in (a) denote one standard deviation, and are symmetric, despite the appearance in log scale, see ref. ⁶⁴. Correspondence between seismic moment M and magnitude m is also provided.

fm	$N_{>fm}$	$N_{<fm}$	N_{fm}	N_{fm}^{pre}	$b_{>fm}$	$b_{<fm}$	b_{fm}	b_{fm}^{pre}
wald								
No: $-135^\circ \leq \rho \leq -45^\circ$	39	5	$N_{no} = 44$	$N_{no}^{pre} = 77$	1.047	—	$b_{no} = 1.081$	$b_{no}^{pre} = 1.484$
Th: $45^\circ \leq \rho \leq 135^\circ$	9	8	$N_{th} = 17$	$N_{th}^{pre} = 77$	—	—	$b_{th} = 0.929$	$b_{th}^{pre} = 0.899$
SS: the rest	461	38	$N_{ss} = 499$	$N_{ss}^{pre} = 503$	0.914	0.726	$b_{ss} = 0.896$	$b_{ss}^{pre} = 0.960$
hernandez								
No: $-135^\circ \leq \rho \leq -45^\circ$	38	3	$N_{no} = 41$	$N_{no}^{pre} = 78$	0.995	—	$b_{no} = 1.011$	$b_{no}^{pre} = 1.502$
Th: $45^\circ \leq \rho \leq 135^\circ$	7	10	$N_{th} = 17$	$N_{th}^{pre} = 61$	—	—	$b_{th} = 0.929$	$b_{th}^{pre} = 0.899$
SS: the rest	420	49	$N_{ss} = 469$	$N_{ss}^{pre} = 506$	0.920	0.840	$b_{ss} = 0.911$	$b_{ss}^{pre} = 0.957$
bbcal								
No: $-135^\circ \leq \rho \leq -45^\circ$	22	4	$N_{no} = 26$	$N_{no}^{pre} = 80$	1.128	—	$b_{no} = 1.165$	$b_{no}^{pre} = 1.521$
Th: $45^\circ \leq \rho \leq 135^\circ$	7	5	$N_{th} = 12$	$N_{th}^{pre} = 69$	—	—	$b_{th} = 1.309$	$b_{th}^{pre} = 0.831$
SS: the rest	280	73	$N_{ss} = 353$	$N_{ss}^{pre} = 507$	0.970	0.886	$b_{ss} = 0.951$	$b_{ss}^{pre} = 0.958$
surfrup								
No: $-135^\circ \leq \rho \leq -45^\circ$	46	5	$N_{no} = 51$	$N_{no}^{pre} = 76$	0.939	—	$b_{no} = 0.966$	$b_{no}^{pre} = 1.470$
Th: $45^\circ \leq \rho \leq 135^\circ$	9	11	$N_{th} = 20$	$N_{th}^{pre} = 61$	—	1.010	$b_{th} = 0.886$	$b_{th}^{pre} = 0.899$
SS: the rest	493	52	$N_{ss} = 545$	$N_{ss}^{pre} = 504$	0.888	0.844	$b_{ss} = 0.884$	$b_{ss}^{pre} = 0.961$

Table 3. Number of events and b -values corresponding to Landers aftershocks with $m \geq 3$ separated by sign of the Coulomb-stress increase ($>$ and $<$) and by focal mechanism (fm) for each slip model. $fm = no$ (normal), ss (strike-slip), and th (thrust). The Coulomb stress is calculated with $\mu' = 0.4$. Same data as in previous tables. Values of b calculated with 10 or less events are not reported. Values for the 5 years previous to Landers are also included and labelled by the superscript pre .

provided by the YHS catalog, the nodal plane in which the Coulomb stress increase is maximum is selected for each aftershock⁴⁹. The results obtained through this procedure are shown in the Supplementary Material.

Influence of focal mechanism. As mentioned in the introduction, some authors have unveiled a direct dependence of the b -value on the focal mechanism of the events, which implies a dependence of b on the total stress (not the stress increase)³⁰. The rake angle is associated to the focal mechanism in the following way: values of the rake around -90° correspond to normal events (labelled as no), values around 0° or $\pm 180^\circ$ to strike-slip events (ss), and values around 90° to thrust events (th). We do not find any significant effect of the rake on the b -value (see Table 3), due to the low number of events in the normal and thrust regimes (which increases the uncertainty). But despite the large uncertainty, the values of b_{no} and b_{ss} are roughly in agreement with the results

of ref. ³⁰; however, our value of b_{th} turns out to be rather large in comparison (similar to b_{ss} but compatible also with b_{no} , within the error bars).

We further observe that ratios $N_{>ss}/N_{<ss}$ and $N_{>no}/N_{<no}$ are higher than $N_{>th}/N_{<th}$; i.e., in strike-slip and normal events the contribution from $\Delta CFS > 0$ is higher than in thrust events, as can be verified looking at Table 3. Comparing with the number of earthquakes with each focal mechanism for the 5 years previous to Landers we conclude that it is indeed the low number of thrust aftershocks with positive ΔCFS which is anomalous (and not the relatively high number of them for negative ΔCFS), due to an increase in the number of normal events and an even higher increase in strike-slip events triggered ($\Delta CFS > 0$) by the Landers mainshock. This difference in numbers becomes visually apparent in Figs. 2, 3 and 4.

Discussion

We have seen how the positive Coulomb-stress increase associated to the Landers mainshock triggered a very large number of strike-slip events and also a large number of normal events, but much less thrust events. Although this result seems easy to establish, as it can be obtained without the calculation of ΔCFS (due to the fact that most of the events have $\Delta CFS > 0$ and thus, this subset dominates the overall statistics), we have unambiguously associated these events to the positive ΔCFS . On the other side, the events in the opposite regime (with $\Delta CFS < 0$) keep a proportion between normal, strike-slip, and thrust events rather different to the $\Delta CFS > 0$ case, and close to that of the immediately previous record (1987–1992, up to Landers). These results are largely independent on the slip model used to calculate the change in Coulomb stress. We have also found that the b -values of the Gutenberg-Richter law for which the Landers event yielded a positive ΔCFS (with $b_{>} \simeq 0.93$) are in general larger than the b -values for the events with negative ΔCFS ($b_{<} \simeq 0.87$); nevertheless, this difference is not statistically significant for any of the slip models used to compute the change in the Coulomb stress.

A non-significant result teaches us that the differences in b -values may be spurious and that certainly, more careful research is necessary in order to overcome statistical limitations. We urge the study of other aftershock sequences for which both knowledge of focal mechanisms as well as detailed slip models for the mainshock are available. It may happen, as for the Landers sequence, that the restrictions in space, time, magnitude, and Coulomb-stress change are too many to yield significant results (in our case, the restriction $m \geq 3$ is particularly strong, but necessary for the fulfillment of the Gutenberg-Richter law). In such a case of low statistics, aggregation (stacking) of sequences from different mainshocks could reduce statistical uncertainty and lead to significant results. This is left for future research.

In addition, a number of extensions and improvements could be incorporated to our approach. We make use of slip models with relatively low resolution in space; so, it would be interesting to know if higher resolution slip models^{79,80} lead to somewhat different values of the strain and the stress, in particular close to the fault. Also, some authors have argued that real faults should have rather low values of the μ' coefficient⁸¹. We provide some check of this in the Supplementary Material, which leads to the conclusion that μ' has little influence on the b -values. Further, in our temporal window of 100 days, the effect of viscoelastic relaxation⁸² should be important; so, this would need to be incorporated into the calculation of the stress. Perhaps more relevant but easier to implement would be the contribution to the stress of the triggered events⁸³. Knowing the focal mechanism of each of these events allows us to calculate the slip direction, which, together with an estimation of the slip value from the magnitude, can be considered an elementary slip model. From this, the event's contribution to the strain can be computed in the same way as for the mainshock. Moreover, we could take into account the relation between b -values and differential stress⁸⁴.

Finally, in a preliminary analysis we have seen that there is no substantial difference in the fulfilling of the Omori law^{33–35} in the two populations of events ($\Delta CFS > 0$ and < 0). Indeed, if we compare this for the two subsets we find the "characteristic" power-law Omori decay of the rate with very similar values of the Omori exponent. Note that this is in disagreement with the rate-and-state formulation²², which does not predict Omori behavior in the case of negative ΔCFS , but instead, contemplates a sudden reduction of seismicity followed by a gradual recovery. The issues discussed in this paper about the Gutenberg-Richter law are equally important in relation to the Omori law. Further research in the lines we point to would be of great interest⁸⁵.

Methods

The YHS catalog characterizes fault planes and slip vectors by means of three angles: strike Θ , dip δ , and rake ρ . In term of these, the normal vector of the fault is given by

$$\hat{n} = \begin{pmatrix} n_E \\ n_N \\ n_U \end{pmatrix} = \begin{pmatrix} \cos\Theta\sin\delta \\ -\sin\Theta\sin\delta \\ \cos\delta \end{pmatrix} \quad (8)$$

in the ENU coordinate system⁸⁶. In the same way, the slip vector is obtained as

$$\hat{\ell} = \begin{pmatrix} \ell_E \\ \ell_N \\ \ell_U \end{pmatrix} = \begin{pmatrix} \sin\Theta\cos\rho - \cos\Theta\cos\delta\sin\rho \\ \cos\Theta\cos\rho + \sin\Theta\cos\delta\sin\rho \\ \sin\delta\sin\rho \end{pmatrix}. \quad (9)$$

Note that \hat{n} and $\hat{\ell}$ are unit vectors.

Received: 11 January 2019; Accepted: 28 January 2020;

Published online: 19 February 2020

References

- Jordan, T. H. *et al.* Operational Earthquake Forecasting. State of knowledge and guidelines for utilization. *Annals Geophys.* **54** (2011).
- Werner, M. *et al.* Retrospective evaluation of time-dependent earthquake forecast models during the 2010–12 Canterbury, New Zealand, earthquake sequence. In *Proceedings of the SSA Annual Meeting, Pasadena (USA)* (2015).
- Michael, A. J. & Werner, M. Preface to the focus section on the Collaboratory for the Study of Earthquake Predictability (CSEP): New results and future directions. *Seism. Res. Lett.* **89**, 1226 (2018).
- Cattania, C. *et al.* The forecasting skill of physics-based seismicity models during the 2010–2012 Canterbury, New Zealand, earthquake sequence. *Seism. Res. Lett.* **89**, 1238 (2018).
- Stein, R., King, G. & Lin, J. Change in failure stress on the southern San Andreas fault system caused by the 1992 magnitude = 7.4 Landers earthquake. *Science* **258**, 1328–1332 (1992).
- King, G., Stein, R. S. & Lin, J. Static stress changes and the triggering of earthquakes. *Bull. Seismol. Soc. Am.* **84**, 935–953 (1994).
- Steady, S., Gombert, J. & Cocco, M. Introduction to special section: stress transfer, earthquake triggering, and time-dependent seismic hazard. *J. Geophys. Res.* **110**, B05S01 (2005).
- Nandan, S., Ouillon, G., Woessner, J., Sornette, D. & Wiemer, S. Systematic assessment of the static stress triggering hypothesis using interearthquake time statistics. *J. Geophys. Res.: Solid Earth* **121**, 1890–1909 (2016).
- Ishibe, T. *et al.* Correlation between Coulomb stress imparted by the 2011 Tohoku-Oki earthquake and seismicity rate change in Kanto, Japan. *Geophys. J. Int.* **201**, 112–134 (2015).
- Segall, P., Llenos, A. L., Yun, S.-H., Bradley, A. M. & Syracuse, E. M. Time-dependent dike propagation from joint inversion of seismicity and deformation data. *J. Geophys. Res.: Solid Earth* **118**, 5785–5804 (2013).
- Cesca, S. *et al.* The 2013 September–October seismic sequence offshore Spain: a case of seismicity triggered by gas injection? *Geophys. J. Int.* **198**, 941–953 (2014).
- Shirzaei, M., Ellsworth, W. L., Tiampo, K. F., González, P. J. & Manga, M. Surface uplift and time-dependent seismic hazard due to fluid injection in Eastern Texas. *Science* **353**, 1416–1419 (2016).
- Quigley, M. C., Jiménez, A., Duffy, B. & King, T. R. Physical and statistical behavior of multifault earthquakes: Darfield earthquake case study, New Zealand. *J. Geophys. Res. Solid Earth* **124**, 4788–4810 (2019).
- Parsons, T., Toda, S., Stein, R. S., Barka, A. & Dietrich, J. H. Heightened odds of large earthquakes near Istanbul: An interaction-based probability calculation. *Science* **288**, 661–665 (2000).
- Hardebeck, J. L., Nazareth, J. J. & Hauksson, E. The static stress change triggering model: Constraints from two southern California aftershock sequences. *J. Geophys. Res.* **103**(24), 427–24,437 (1998).
- Marsan, D. Triggering of seismicity at short timescales following Californian earthquakes. *J. Geophys. Res.* **108**, 1–14 (2003).
- Mallman, E. P. & Zoback, M. D. Assessing elastic Coulomb stress transfer models using seismicity rates in southern California and southwestern Japan. *J. Geophys. Res.: Solid Earth* **112** (2007).
- Felzer, K. R. & Brodsky, E. E. Testing the stress shadow hypothesis. *J. Geophys. Res.: Solid Earth*, **110** (2005).
- Gutenberg, B. & Richter, C. F. Frequency of earthquakes in California. *Bull. Seismol. Soc. Am.* **34**, 185–188 (1944).
- Utsu, T. Representation and analysis of earthquake size distribution: a historical review and some new approaches. *Pure Appl. Geophys.* **155**, 509–535 (1999).
- Kagan, Y. Y. *Earthquakes: Models, Statistics, Testable Forecasts*. Wiley (2014).
- Dieterich, J. A constitutive law for rate of earthquake production and its application to earthquake clustering. *J. Geophys. Res.: Solid Earth* **99**, 2601–2618 (1994).
- Toda, S., Stein, R., Richards-Dinger, K. & Bozkurt, S. Forecasting the evolution of seismicity in Southern California: Animations built on earthquake stress transfer. *J. Geophys. Res.* **110**, B05S16 (2005).
- Chan, C. H., Wu, Y. M. & Wang, J. P. Earthquake forecasting through a smoothing kernel and the rate-and-state friction law: Application to the Taiwan region. *Nat. Hazards Earth Syst. Sci.* **12**, 1–13 (2012).
- Cattania, C., Hainzl, S., Wang, L., Roth, F. & Enescu, B. Propagation of Coulomb stress uncertainties in physics-based aftershock models. *J. Geophys. Res.* **119**, 7846–7864 (2014).
- Cattania, C., Hainzl, S., Wang, L., Enescu, B. & Roth, F. Aftershock triggering by postseismic stresses: A study based on Coulomb rate-and-state models. *J. Geophys. Res.* **120**, 2388–2407 (2015).
- Seeber, L. & Armbruster, J. G. Earthquakes as beacons of stress change. *Nature* **407**, 69–72 (2000).
- Dieterich, J., Cayol, V. & Okubo, P. The use of earthquake rate changes as a stressmeter at Kilauea volcano. *Nature* **408**, 457–460 (2000).
- Kamer, Y. & Hiemer, S. Data-driven spatial *b* value estimation with applications to California seismicity: To *b* or not to *b*. *J. Geophys. Res.* **120**, 5191–5214 (2015).
- Schorlemmer, D., Wiemer, S. & Wyss, M. Variations in earthquake-size distribution across different stress regimes. *Nature* **437**, 539–542 (2005).
- Narteau, C., Byrdina, S., Shebalin, P. & Schorlemmer, D. Common dependence on stress for the two fundamental laws of statistical seismology. *Nature* **462**, 642–645 (2009).
- Gulia, L. & Wiemer, S. Real-time discrimination of earthquake foreshocks and aftershocks. *Nature* **574**, 193–199 (2019).
- Omori, F. On the aftershocks of earthquakes. *J. Coll. Sci. Imp. Univ. Tokyo* **7**, 111–200 (1894).
- Utsu, T. A statistical study of the occurrence of aftershocks. *Geophys. Mag.* **30**, 521–605 (1961).
- Utsu, T., Ogata, Y. & Matsu'ura, R. The centenary of the Omori formula for a decay law of aftershock activity. *J. Phys. Earth* **43**, 1–33 (1995).
- Wyss, M. & Wiemer, S. Change in the probability for earthquakes in southern California due to the Landers magnitude 7.3 earthquake. *Science* **290**, 1334–1338 (2000).
- Kanamori, H. & Brodsky, E. E. The physics of earthquakes. *Rep. Prog. Phys.* **67**, 1429–1496 (2004).
- Hill, D. P. *et al.* Seismicity remotely triggered by the magnitude 7.3 Landers, California, earthquake. *Science* **260**, 1617–1623 (1993).
- Hauksson, E., Jones, L. M., Hutton, K. & Eberhart-Phillips, D. The 1992 Landers earthquake sequence: Seismological observations. *J. Geophys. Res.: Solid Earth* **98**, 19835–19858 (1993).
- Gombert, J., Reasenber, P. A., Bodin, P. & Harris, R. A. Earthquake triggering by seismic waves following the Landers and Hector Mine earthquakes. *Nature* **411**, 462–466 (2001).
- Wald, D. J. & Heaton, T. H. Spatial and temporal distribution of slip for the 1992 Landers, California, earthquake. *Bull. Seismol. Soc. Am.* **84**, 668–691 (1994).
- Hernandez, B., Cotton, F. & Campillo, M. Contribution of radar interferometry to a two-step inversion of the kinematic process of the 1992 Landers earthquake. *J. Geophys. Res. Solid Earth* **104**, 13083–13099 (1999).
- Steady, S., Marsan, D., Nalbant, S. S. & McCloskey, J. Sensitivity of static stress calculations to the earthquake slip distribution. *J. Geophys. Res. Solid Earth*, **109** (2004).
- Spotila, J. A. & Sieh, K. Geologic investigations of a "slip gap" in the surficial ruptures of the 1992 Landers earthquake, Southern California. *J. Geophys. Res. Solid Earth* **100**, 543–559 (1995).
- Hauksson, E., Yang, W. & Shearer, P. M. Waveform relocated earthquake catalog for Southern California (1981 to June 2011.). *Bull. Seismol. Soc. Am.* **102**, 2239–2244 (2012).
- Kamer, Y., Ouillon, G., Sornette, D. & Woessner, J. Condensation of earthquake location distributions: Optimal spatial information encoding and application to multifractal analysis of South Californian seismicity. *Phys. Rev. E* **92**, 022808 (2015).

47. Yang, W., Hauksson, E. & Shearer, P. M. Computing a large refined catalog of focal mechanisms for Southern California (1981–2010): Temporal stability of the style of faulting. *Bull. Seismol. Soc. Am.* **102**, 1179–1194 (2012).
48. Hardebeck, J. L. & Shearer, P. M. A new method for determining first-motion focal mechanisms. *Bull. Seism. Soc. Am.* **92**, 2264–2276 (2002).
49. Strader, A. & Jackson, D. D. Near-prospective test of Coulomb stress triggering. *J. Geophys. Res.: Solid Earth* **119**, 3064–3075 (2014).
50. Okada, Y. Internal deformation due to shear and tensile faults in a half-space. *Bull. Seismol. Soc. Am.* **82**, 1018–1040 (1992).
51. Battaglia, M., Cervelli, P. F. & Murray, J. R. dMODELS: A MATLAB software package for modeling crustal deformation near active faults and volcanic centers. *J. Volcanol. Geotherm. Res.* **254**, 1–4 (2013).
52. Lautrup, B. *Physics of Continuous Matter*, CRC Press, 2nd edn. (2011).
53. McCloskey, J. *et al.* Structural constraints on the spatial distribution of aftershocks. *Geophys. Res. Lett.* **30**, 1610–1613 (2003).
54. Ishibe, T., Ogata, Y., Tsuruoka, H. & Satake, K. Testing the Coulomb stress triggering hypothesis for three recent megathrust earthquakes. *Geosci. Lett.* **4** (2017).
55. Aki, K. & Richards, P. G. *Quantitative seismology* University Science Books (2002).
56. Vavryčuk, V. Earthquake mechanisms and stress field. In Beer, M., Kougiumtzoglou, I. A., Patelli, E. & Au, I. S.-K. (eds.) *Encyclopedia of earthquake engineering*, (Springer-Verlag, Berlin 2015).
57. Cocco, M. & Rice, J. R. Pore pressure and poroelasticity effects in Coulomb stress analysis of earthquake interactions. *J. Geophys. Res.: Solid Earth* (2002).
58. Stein, R. S. The role of stress transfer in earthquake occurrence. *Nature* **402**, 605–609 (1999).
59. Aki, K. Maximum likelihood estimate of b in the formula $\log N = a - bm$ and its confidence limits. *Bull. Earthq. Res. Inst. Univ. Tokyo* **43**, 237–239 (1965).
60. Marzocchi, W. & Sandri, L. A review and new insights on the estimation of the b -value and its uncertainty. *Annals Geophys.* **46**, 1271–1282 (2009).
61. Bender, B. Maximum likelihood estimation of b -values for magnitude grouped data. *Bull. Seism. Soc. Am.* **73**, 831–851 (1983).
62. Press, W. H., Teukolsky, S. A., Vetterling, W. T. & Flannery, B. P. *Numerical Recipes in FORTRAN*. Cambridge University Press, Cambridge, 2nd edn. (1992).
63. Clauset, A., Shalizi, C. R. & Newman, M. E. J. Power-law distributions in empirical data. *SIAM Rev.* **51**, 661–703 (2009).
64. Deluca, A. and Corral, A. Fitting and goodness-of-fit test of non-truncated and truncated power-law distributions. *Acta Geophys.* **61**, 1351–1394 (2013).
65. Corral, A. & Gonzalez, A. Power law size distributions in geoscience revisited. *Earth Space Sci.* **6**, 673–697 (2019).
66. Woessner, J. & Wiemer, S. Assessing the quality of earthquake catalogues: Estimating the magnitude of completeness and its uncertainty. *Bull. Seismol. Soc. Am.* **95**, 684–698 (2005).
67. Shi, Y. & Bolt, B. A. The standard error of the magnitude-frequency b value. *Bull. Seismol. Soc. Am.* **72**, 1677–1687 (1982).
68. Pawitan, Y. *In All Likelihood: Statistical Modelling and Inference Using Likelihood*. Oxford UP, Oxford (2001).
69. Good, P. I. *Resampling Methods*. Birkhäuser, Boston, 3rd edn. (2011).
70. Anderson, K. P. B. D. R. *Model Selection and Multimodel Inference*. Springer-Verlag New York (2002).
71. Reasenber, P. A. & Jones, L. M. Earthquake hazard after a mainshock in California. *Science* **243**, 1173–1176 (1989).
72. Jones, L. M. Foreshocks, aftershocks, and earthquake probabilities: Accounting for the Landers earthquake. *Bull. Seismol. Soc. Am.* **84**, 892 (1994).
73. Hutton, K., Woessner, J. & Hauksson, E. Earthquake monitoring in Southern California for seventy-seven years (1932–2008.). *Bull. Seismol. Soc. Am.* **100**, 423 (2010).
74. Shcherbakov, R., Turcotte, D. L. & Rundle, J. B. Aftershock statistics. *Pure Appl. Geophys.* **162**, 1051–1076 (2005).
75. Hernandez, S., Brodsky, E. E. & van der Elst, N. J. The magnitude distribution of dynamically triggered earthquakes. *Geochem. Geophys. Geosys.* **15**(9), 3688–3697 (2014).
76. Navas-Portella, V., Serra, I., Corral, A. & Vives, E. Increasing power-law range in avalanche amplitude and energy distributions. *Phys. Rev. E* **97**, 022134 (2018).
77. Corral, A., Boleda, G. & Ferrer-i-Cancho, R. Zipf's law for word frequencies: Word forms versus lemmas in long texts. *PLoS ONE* **10**, e0129031 (2015).
78. Murtaugh, P. A. In defense of p values. *Ecology* **95**, 611–617 (2014).
79. Olsen, K. B., Madariaga, R. & Archuleta, R. J. Three-Dimensional Dynamic Simulation of the 1992 Landers Earthquake. *Science* **278**(5339), 834–838 (1997).
80. Peyrat, S., Olsen, K. & Madariaga, R. *Dynamic modeling of the 1992 Landers earthquake*. *J. of Geo. Res.: Solid Earth* **106**(B11), 26467–26482 (2001).
81. Mulargia, F. & Bizzarri, A. Earthquake friction. *Physics of the Earth and Planetary Interiors* **261**, 118–123 (2016).
82. Sabadini, R., Vermeersen, B. & Cambiotti, G. *Global Dynamics of the Earth*. 2nd Edition, Springer (2016).
83. Felzer, K. R., Abercrombie, R. E. & Ekström, G. Secondary Aftershocks and Their Importance for Aftershock Forecasting. *Bull. Seism. Soc. Am.* **93**, 1433–1448 (2003).
84. Amitrano, D. Brittle-ductile transition and associated seismicity: Experimental and numerical studies and relationship with the b value. *J. Geophys. Res.: Solid Earth* **108** (2003).
85. Kagan, Y. Y. Earthquake size distribution: Power-law with exponent $\beta \equiv 1/2$? *Tectonophysics* **490**, 103–114 (2010).
86. Smith, D. E. *A new paradigm for interpreting stress inversions from focal mechanisms: how 3D stress heterogeneity biases the inversions toward the stress rate*. Ph.D. thesis, school California Institute of Technology (2006).

Acknowledgements

We are grateful to Álvaro González for some comments on the manuscript, to Paolo Gasperini, Francesco Mulargia, Fabio Romanelli and Roberto Sabadini for the feedback provided during the International Workshop on Seismic Source Physics, Sardinia, and to two anonymous referees who detected some problems in a previous version of the manuscript. The research leading to these results has received funding from "La Caixa" Foundation. V. N. acknowledges financial support from the Spanish Ministry of Economy and Competitiveness (MINECO, Spain), through the "María de Maeztu" Program for Units of Excellence in R & D (Grant No. MDM-2014-0445). We also acknowledge financial support from MINECO and MICIU under Grants No. FIS2015-71851-P, FIS-PGC2018-099629-B-I00, and "Proyecto Redes de Excelencia" Grant No. MAT2015-69777-REDT. A. J. appreciates the hospitality of the Centre de Recerca Matemàtica.

Author contributions

V.N.-P. and A.J. performed the computations, A.J. and A.C. wrote the manuscript. All authors discussed the results and reviewed the manuscript.

Competing interests

The authors declare no competing interests.

Additional information

Supplementary information is available for this paper at <https://doi.org/10.1038/s41598-020-59416-2>.

Correspondence and requests for materials should be addressed to Á.C.

Reprints and permissions information is available at www.nature.com/reprints.

Publisher's note Springer Nature remains neutral with regard to jurisdictional claims in published maps and institutional affiliations.



Open Access This article is licensed under a Creative Commons Attribution 4.0 International License, which permits use, sharing, adaptation, distribution and reproduction in any medium or format, as long as you give appropriate credit to the original author(s) and the source, provide a link to the Creative Commons license, and indicate if changes were made. The images or other third party material in this article are included in the article's Creative Commons license, unless indicated otherwise in a credit line to the material. If material is not included in the article's Creative Commons license and your intended use is not permitted by statutory regulation or exceeds the permitted use, you will need to obtain permission directly from the copyright holder. To view a copy of this license, visit <http://creativecommons.org/licenses/by/4.0/>.

© The Author(s) 2020